

EXPERIMENTS WITH ELECTRON CLOUD AND SOURCES

M. Cavenago*, INFN-LNL, Legnaro, Italy; G. Bettega, F. Cavaliere,
D. Ghezzi, A. Illiberi, R. Pozzoli, M. Romé, INFN-Milano and Univ. Milano, Italy

Abstract

The Penning-Malmberg trap ELTRAP installed at University of Milan can provide electron clouds of several sizes for studies of non-linear physics: length ranges from 0.15 to 1 m, while diameter is varied between 25 mm and 70 mm by changing the electron source: filament or planar spiral. Slow instabilities, due to the accumulation of ions inside the trap are observed and cured by clearing fields. A theory of bunching due to injection voltage is presented and some preliminary evidences discussed. Plan to install a third laser modulated electron source and additional diagnostic are also summarized.

INTRODUCTION

The electron trap ELTRAP (installed at the University of Milan [1]) is a Penning Malmberg trap for the storage of electron clouds, for studies in nonlinear dynamics and accelerator physics. As well known, pure electron plasmas can reach confinement times τ_i in the order of 100 s, so that evolution of several plasma structures can be observed[2]. In some conditions, we observed typical instability of the plasma column, related to ion presence and correlated to the speed of injection process; we developed some stabilization techniques[3]. A simple theory of the effect of injection is presented here, with experiments devoted to isolate the bunching or the oscillations induced.

Interest of analogy of the vortices of electron plasma confined in Penning Malmberg traps with several dynamical systems, with application spanning from meteorology to astrophysics to superconductivity to high intensity particle accelerators are well known and described elsewhere[2]. Let us remember also three practical applications of Penning based devices: ion pumps, ion sources[4] and storage of ions of exotic nuclei.

Fig. 1 shows a partial scheme of the Eltrap machine. A 1.5 m long solenoid with axis z generates a very uniform magnetic field ($\Delta B_z/B_z < 0.0005$ for $|z| < 0.5$ m, with careful placing of iron shims at the ends). At about $z = -0.55$ m an electron source with central potential V_b is immersed in the magnetic field, while a phosphor screen P is placed at $z = 0.6$ m, with a potential V_p ; typically $V_b = -60$ to -7 V and $V_p = +3$ kV with respect to vacuum chamber $\phi = 0$. In between, there are 9 cylindrical electrodes C0, C1, etcetera with inner radius $r_w = 4.5$ cm, whose potential $V_i(t)$ can be arbitrarily programmed in time with a special function generator $|V_i| \leq 100$ V; we have also two sectored electrode sets S2, S4. Detail of the ELTRAP recent upgrade with a planar source are given in

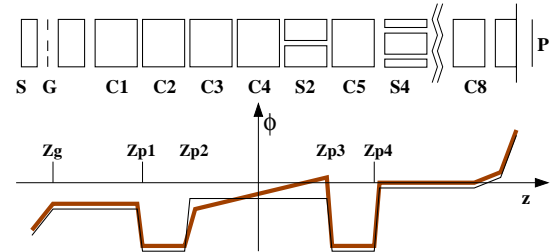


Figure 1: Scheme of ELTRAP electrodes when plasma is trapped between C2 and C5; potential ϕ takes space charge into account and thicker line is the 'clearing field' case.

a separate section; an external source was also completed, while an external beam dump is being designed for use of laser diagnostics.

A few basic operation mode of the ELTRAP machine can be identified: a) beam regime, where all $V_i \cong 0$; the electron drift freely from source to phosphor, with vorticity evolution proportional to v_z/B_z and virtual cathode formation at beam center $r = 0$ [5]; b) beam plasma regime, with $V_7 = -80$ V, so that electrons are reflected back to the source and exit through the filament spacing; c) injection-hold-extraction cycle. At injection $V_7 = -80$ V, so that two counter-moving streams of electrons fill the trap; then also V_2 is turned on $V_2 = -80$ V, so that escaping electrons are reflected back into the trap at z_{p2} ; this is the hold (or trapped) phase; after a programmed time t_h , V_7 is turned off, so that electrons may approach the phosphor where they are drastically accelerated. Electrodes C_2 and C_7 here act as gates or plug electrodes, and their role can of course be assigned to any other electrodes C_i and C_h , so that trapped plasma length can be changed.

Some 'ion-driven' instabilities [3] were related to the ramp rate R_v of electrode C_2 voltage V_2 and stabilized with 'clearing fields': $R_v = dV_2/dt \leq 300$ kV/ms. A simply single particle theory of the V_2 bunching effect is given in the next section, while a summary of 'clearing fields' results, experimental evidences of bunching and its measuring techniques are discussed in the last section.

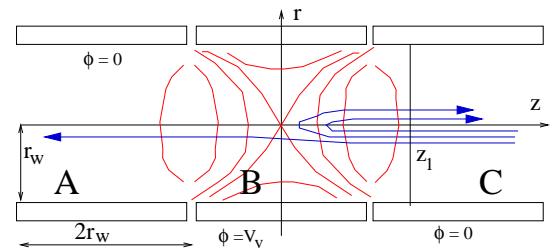


Figure 2: Model geometry: the pulsed electrode B reflects the beam; some equipotentials and e^- paths (arrows) are shown.

*cavenago@lnl.infn.it

BEAM REFLECTION

The simplified geometry used in this section is shown in fig 2; here $z = 0$ is the plug electrode B , to which a voltage $V_v = -R_v t$ for $t \geq 0$ is applied; $V_v = 0$ for $t < 0$. Other electrodes are grounded; from electrostatic simulation we see that ϕ is well approximated by a series expansion $\phi_b = V_v(t)[a_0 + a_2(\frac{1}{4}r^2 - \frac{1}{2}z^2) + \dots]$ near B and is almost zero otherwise, so that $\phi = \min(\phi_b, 0)$ gives an approximate map of most equipotentials, with $a_0 = 0.866$ and $a_2 \cong 400/\text{m}^2$. Since electron motion is magnetized, r is frozen. In the limit $B_z \rightarrow \infty$, the Hamiltonian for z is $H = p_z^2/(2m) + e\varphi$ with $\varphi(z) = -\phi(r, z)$. In detail, we have

$$\varphi(z) = \max[0, r_v t(1 - \alpha z^2)] \quad (1)$$

where r_v and α are constants; for example, when $r = 0$, we have $r_v = a_0 R_v = 250 \text{ kV/ms}$ and $\alpha = a_2/(2a_0)$. Let $z_1 = 1/\sqrt{\alpha} = 65 \text{ mm}$. For $|z| > z_1$ or $t < 0$ the motion is inertial. For $|z| \leq z_1$ and $t \geq 0$ the motion equation $\ddot{z} = k_1 t z$ with $k_1 = 2r_v \alpha e/m$ is solved as

$$z(t) = c_1 \text{Ai}(k_2 t) + c_2 \text{Bi}(k_2 t), \quad k_2 = (k_1)^{1/3} = 46 \text{ MHz} \quad (2)$$

with Ai, Bi Airy functions. It is convenient to scale variables as $s = z/z_1$ and $\lambda = k_2 t$, so that $s'(\lambda) = v_z/(k_2 z_1)$. By chance, $s' = 1$ corresponds $v_z = 3 \times 10^6 \text{ m/s}$, that is a kinetic energy of 25 eV. To fix ideas, the electron arrives from $s > 1$ side; let λ_i be the time when it enters in the plug $s = 1$, and λ_f when it returns at $s = 1$. Let $I_0 = -s'(\lambda_i) = |v_z(t_i)|/k_2 z_1$ be the input parameter and $\mathcal{G}(\lambda, \lambda_i) = \pi[\text{Bi}(\lambda)\text{Ai}(\lambda_i) - \text{Ai}(\lambda)\text{Bi}(\lambda_i)]$ a convenient function, so that motion is

$$s(\lambda) = -\mathcal{G}_{01} - I_0 \mathcal{G} \quad \text{with} \quad \mathcal{G}_{mn} = (\partial_\lambda)^m (\partial_{\lambda_i})^n \mathcal{G} \quad (3)$$

Note the identities $\mathcal{G}_{20} = \lambda \mathcal{G}$ and $\mathcal{G}\mathcal{G}_{11} - \mathcal{G}_{10}\mathcal{G}_{01} = 1$. The exit parameters $F_0 = s'(\lambda_f)$ and λ_f are determined by

$$F_0 = (\mathcal{G}_{10} - 1)/\mathcal{G}(\lambda_f, \lambda_i) \quad , \quad I_0 = -(\mathcal{G}_{01} + 1)/\mathcal{G}(\lambda_f, \lambda_i) \quad (4)$$

and λ_f exists if $I_0 < -\text{Ai}'(\lambda_i)/\text{Ai}(\lambda_i)$. On the reflected particle path (a ray)

$$s(\lambda) = 1 + (\lambda - \lambda_f)F_0 \quad , \quad (5)$$

the density is $n_e = n_0 I_0 / |ds/d\lambda_i|$ where n_0 is the density of the input beam and $ds/d\lambda_i = (\lambda - \lambda_f)(dF_0/d\lambda_i) - F_0(d\lambda_f/d\lambda_i)$ with the expressions for

$$\frac{d\lambda_f}{d\lambda_i} = -\frac{\lambda_i \mathcal{G} + I_0 \mathcal{G}_{01}}{\mathcal{G}_{11} + I_0 \mathcal{G}_{10}} \quad (6)$$

and for the F_0 total derivative. From fig 3 we see that two initial λ_i , named $\lambda_i^\pm(s, \lambda)$, correspond to a (s, λ) , where the second is due to a slow component. Therefore two n_e contributions are summed in the density, as singular as $(s_m - s)^{-1/2}$ at the front $s \leq s_m$. The total charge reflected in $s > 1$ is $n_{e0}[\lambda_i^+(s, \lambda) - \lambda_i^-(1, \lambda)]$. Note that, after $\lambda = \lambda_s \cong 15$ when $V_v(t)$ rise stops, minor corrections also applies.

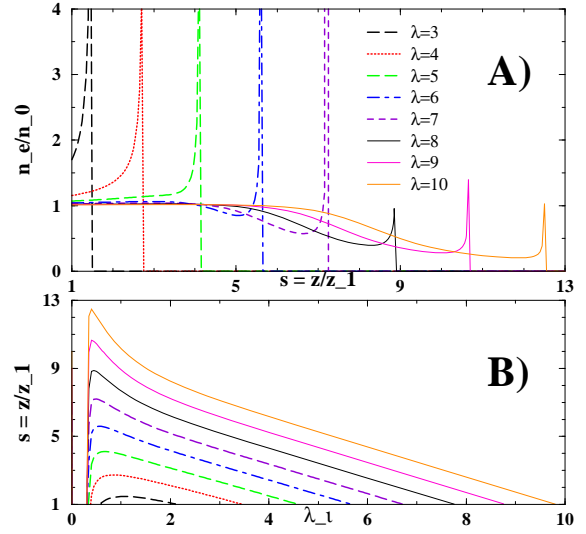


Figure 3: A) Plot of n_e/n_0 vs s at several scaled times λ with $I_0 = 0.9$. B) Plot of s vs λ_i at the same λ values.

SETUP AND UPGRADES

The planar spiral source has a 70 mm diameter and is directly heated by a filament current I_f , with V_f the filament voltage. The test stand vacuum chamber is cooled. In a typical test, see Fig. 4, a voltage $V_b = -20 \text{ V}$ is applied to its center and a voltage $V_c = 15 \text{ V}$ to a collector 20 mm far away. Currents I_b and I_c are measured, and the emitted current is estimated as $I_s = \min(I_b, I_c)$. The conditioning consists in a progressive heating of the spiral up to the sustainable operation current. Some nonuniformity of the spiral temperature was evident during tests at large I_f and later in beam operation in ELTRAP. Since spirals are made of sintered W/Cu, after two cycles at $I_f = 55 \text{ A}$, the first spiral treated became so brittle (for Cu evaporation), that it was broken during dismount from the test assembly. A high temperature furnace to treat several spirals at one time and to improve uniformity is being commissioned. In ELTRAP, current I_f in the second spiral is limited by thermal load consideration (to about 33 A, depending on its mount-

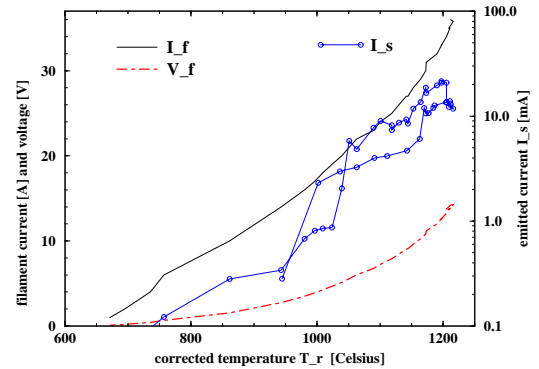


Figure 4: Emission characteristic of the freshly treated second electron spiral source, after its conditioning.

ing), so that only a few mA are envisioned in continuous operation. Still this is an improvement respect the usual 25 mm filament, with $I_s \cong 0.4$ mA. To suppress the magnetic effects of I_f on the plasma, another spiral (in copper) is placed at the rear of the source (as visible in fig 5) and a quadrupole transmission line is used.

Since the external source is to be mounted externally, very tight alignment tolerance are provided. Classical solutions were used for extraction (triode configuration) and focusing (Helmholtz coils). The pulse control uses a pre-heated cathode [6] at a temperature $T_s = 1100$ K where its emission is still negligible; emission is greatly enhanced by the laser pulse, which determines the electron current profile. Effect of longitudinal emittance, of great importance in rf injectors, can be therefore physically simulated.

A more ambitious upgrading initiative, which envisions the use of Thompson scattering from a powerful laser to complete the diagnostic of the coherent structures in the three spatial dimensions, was recently approved (experiment ELTEST, INFN, group 5). In this application it is necessary to replace the phosphor screen with a 0.5 m extension housing the detection photomultipliers and the laser input optics. Moreover the electron beam should be deflected and dumped off axis, which implies additional iron shims of the main solenoid. Design is in progress.

RESULTS

Connecting an electrode, say C_2 , to the inverting input of a differential amplifier (which acts as a virtual ground) and with typical circuitry, a signal $S_2(t)$ proportional to the charge Q_2 induced on that electrode can be obtained. This pickup is highly sensitive to the plasma motion along z , while rotation (coordinate ϑ) is coupled only through higher order effects (misalignments, $r-z$ coupling). An instability (oscillation in S_2) at a typical diocotron frequency (20 to 50 kHz) was observed; see Fig 6. One stabilization technique named 'clearing fields' consists in adding a small $\delta\phi \cong E_0 z$ to electrodes from C_3 to C_6 for some time: instability reduces to zero rapidly. We speculate that these fields push ions into the plug electrodes.

In a set I of experiments, named reflection against pulsed

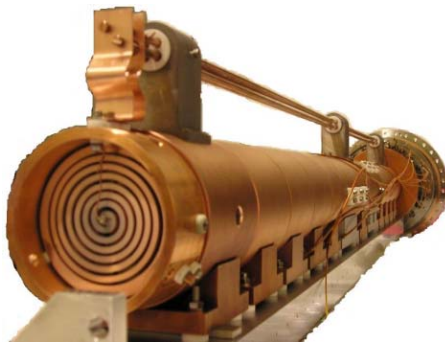


Figure 5: The spiral source aligned with other electrodes of the ELTRAP facility.

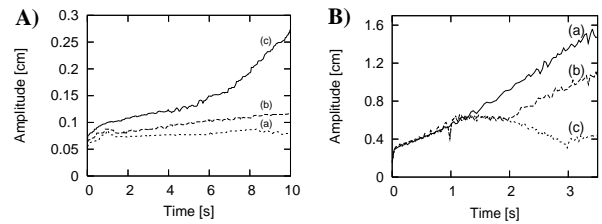


Figure 6: A: Displacement amplitude D of the 'ion-driven' instability vs time, with $V_b = -7$ V and different $R_v = 40$ V/ms (a), 120 V/ms (b), 80 kV/ms (c). B: Displacement amplitude vs time with $V_b = -18$ V and $R_v = 80$ kV/ms and (a) no clearing fields; (b) clearing fields only for $1 < t < 2$ s; (c) clearing fields only for $1 < t < 3$ s.

barrier, electrode C7 was switched on for $3 \mu\text{s}$ (and off for $100 \mu\text{s}$) and C1, C2 were connected to the amplifier and to a 10 Gsample/s Digital Sampling Oscilloscope, to record a $5 \mu\text{s}$ track S_2 , averaged over 100 sweeps. Source voltages $V_b = -30$ V and $V_f = 13.3$ V were held fixed, as well as $B_0 = 500$ G, while several barrier on-voltages V_{o7} were tested. Current emitted from the spiral source is still well visible on phosphor, due to the low duty factor of the barrier. S_2 shows many spurious oscillation.

Therefore in a set II of experiments a static barrier of -80 V was added to electrode C5, to prevent the electron beam to arrive at C7. Net pickup signal, defined as $S_n = S_2(\text{I}) - S_2(\text{II})$, is shown in fig. 7. A non-periodic leading edge, comparable with fig. 3 spikes of n_e , is clearly visible. Results are still preliminary, since more work on amplifiers and on C5 drive signal quality is needed.

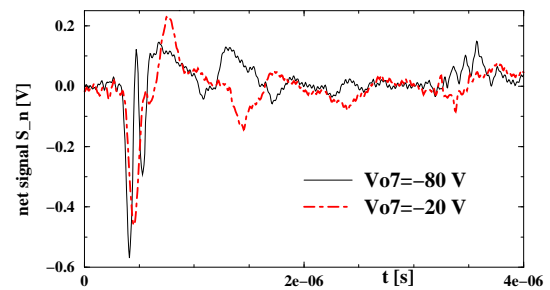


Figure 7: Charge net signal S_n with two V_{o7} voltages.

REFERENCES

- [1] M. Amoretti et al., Rev. Sci. Instrum. **74** (2003) 3991.
- [2] D. H. E. Dubin and T. M. O'Neil, Rev. Modern Physics **71** (1999) 87.
- [3] G. Bettega, F. Cavaliere, M. Cavenago, A. Illiberi, R. Pozzoli, M. Romè, Plasma Phys. Control. Fusion, **47**, (2005) 1697.
- [4] M. Cavenago, A. Galatá, T. Kulevov, S. Petrenko, Rev. Sci. Instrum., **77** (2006), 03A339.
- [5] M. Cavenago et al., Proceeding of the 2004 EPAC (EPAC, Lucerne, 2004), 2083.
- [6] D. W. Feldman et al., Proceeding of the 2001 PAC (IEEE, Piscataway, 2001), 2132.